Chapter 1
Introduction

The very topic discussed here suggests that we are interested in telescopes that combine a large field of view with a high survey speed of sufficiently faint objects. All of these interrelated concepts are largely determined by the goal of the observation.

To estimate the required speed of a sky survey S, as measured in square degrees per second ($\deg^2$/sec), we assume that one needs to cover 10^4 $\deg^2$ of sky in 3 hours. The specified area is a little smaller than the entire hemisphere visible above the horizon and free of absorption in the Milky Way and Earth's light pollution at large zenith angles, so our estimate matches the goals of real sky surveys. The resulting survey speed $S \simeq 1$ $\deg^2$/sec, which indicates that the problem is nontrivial.

Indeed, the field of view of a *classical Cassegrain* telescope (the parabolic primary and hyperbolic secondary mirrors; see Section 2.2.2) is only several arc minutes wide, so one would need to acquire about 10^6 images to cover the required area of sky, which is unrealistic even with multiple telescopes. The Ritchey–Chrétien telescope with both hyperbolic mirrors (Section 2.2.3), recently considered to be a wide-field instrument, also fails to solve the problem. The field of a Ritchey–Chrétien telescope does not exceed approximately $20'$, which might reduce the number of images mentioned above, but only by an order of magnitude. Thus, to perform a typical survey investigation, telescopes with an angular field diameter $2w$ of at least $1°$ are required. Most of the problems mentioned in the Preface need telescopes with a field from a few to tens of degrees in diameter (see Section 4.4.1).

There are two primary modes of surveying large areas of the sky: (i) we need to cover *sequentially* the area in reasonable time; and (ii) the sky area we are interested in should be under *continuous* observation. The problem of the first kind arises, for example, when we study the long-term variability of all objects on the celestial sphere brighter than a certain limit. The second mode is characteristic for cases where we look for fast transient objects, say, the counterpart of an x-ray burst.

The choice of mode is determined by the brightness and the characteristic time of evolution of the events under investigation. Of course, there are also intermediate situations.

In most of the current sky surveys, the faintest objects have about 19–22 magnitude in the visual range, which implies the use of telescopes at least 75 cm in diameter. However, a number of important problems, e.g., tracking asteroids dangerous to the Earth, can be solved with telescopes with a smaller aperture but a significantly wider field of view than conventional field of large instruments. It is rather difficult to set the lower boundary of the aperture dimension of a telescope that is useful as a survey instrument. In particular, interest in multi-lens systems of the type *Evryscope* (Law et al. 2015) with an aperture of about 10 cm is now noticeable. On the other hand, the achievement of a significant field of view with telescopes that have an aperture of more than 10 m is insufficiently studied, so the present discussion is confined to the above upper limit.

1.1 Preliminary Definitions

The variety of goals entails a wide diversity in size, type, and performance of survey telescopes. Before turning to a detailed discussion of the topic, it would be desirable to define the concepts of image quality, field of view, and classification of wide-field telescopes. We will specify these later, but for now it is enough to glance at the total set of wide-field telescopes in operation and those under construction.

1.1.1 Types of telescopes

Single-mirror telescopes are naturally subdivided according to the shape of the mirror surface. In the astronomical aspect, parabolic and spherical mirrors are of particular interest; the former because of the ability to form a diffraction image of an infinitely distant axial source of light (Section 2.1), and the latter due to the simplicity of the surface shape.

Following the common terminology (see, e.g., Schroeder 2000, Section 6.2), we call a Cassegrain system *classical* if its primary is a paraboloid. The *aplanatic Cassegrain* system,[1] or *Ritchey–Chrétien* (RC) telescope, consists of two hyperboloidal mirrors with specific values of eccentricities, which depend upon the layout's first-order parameters according to Eq. (2.16) of Section 2.2.3.

Further, a *Quasi-Ritchey–Chrétien* (QRC) system is a RC telescope with a lens field corrector between the secondary mirror and focal surface. The same term is often applied to similar systems, when both the mirrors and the

1 *Aplanat* is an optical system in which both spherical aberration and coma are corrected.

corrector elements are slightly optimized as a whole, so the purely reflective two-mirror subsystem remains close to the strict RC. In other words, the two-mirror part of a QRC telescope should provide feasible images in the paraxial field.

The deep co-optimization of mirror optics and a lens corrector leads to a system whose parameters differ significantly from those for a QRC. For example, the Pan-STARRS telescope PS1 with a conic constant[2] of a secondary mirror equal to −21.4 cannot be regarded as an RC with a corrector or a QRC, as can be found in the literature. It is convenient to name such systems *Cassegrain telescopes with a corrector* or, for brevity, *corrected Cassegrain* systems.

Terms similar to those used for the Cassegrain system are appropriate for versions generated by a Gregorian system (Section 2.2.2). The *classical* Gregorian telescope has a paraboloidal primary mirror and an ellipsoidal secondary one. The corresponding aplanatic version of the Gregorian system was described for the first time by Maksutov (1932), so we call it the *Gregory–Maksutov* (GM) system (Section 2.2.3). Both mirrors of a GM telescope are ellipsoids, whose conic constants are given by the same Eq. (2.16). Finally, the *corrected Gregorian* telescope includes two mirrors and a lens corrector provided that the parameters of the entire optical system have undergone deep optimization. An example of such a system is given in Section 3.2.4.

We spoke above about single-mirror and two-mirror telescopes. The need to provide a large field of view for telescopes of considerable aperture leads to the development of purely reflective systems with a larger number of mirrors. Section 2.3 discusses only two such systems: the Paul and Korsch three-mirror telescopes. The first of them is a wide-field mirror analogue of the Schmidt camera with a practically plane-parallel beam of light going to the third mirror. The second system, a *three-mirror anastigmat* (TMA), is characterized by the complete elimination of third-order aberrations, which ensures excellent image quality within the field up to 2-3°. The problem of light vignetting, severe even in three-mirror telescopes, becomes critically acute for systems with a larger number of mirrors, which is addressed in the fairly extensive literature.

Adding lens optics to mirrors opens up a variety of catadioptric telescopes, which are discussed in Chapters 3 and 4. These systems are commonly referred to as "the discoverer." The division of catadioptric telescopes according to the number of full-aperture lenses in the input corrector, which is used in Chapter 4, seems to be an adequate approach to the difficult task of classifying these systems.

2 The conic constant is the square of the eccentricity, taken with the opposite sign.

1.1.2 Image quality

It is worth repeating that the angular diameter of the useful field of view $2w$ is determined by the quality of the images in it.[3] The usual way to describe approximately the image quality provided by a telescope is to give the root-mean-square (RMS) angular diameter Δ''_{rms} of a star image in arc seconds (arcsec). It is more likely now to use another parameter, the angular diameter Δ''_{80} of a circle, which contains 80% of the energy in the image of a star. It is also popular in observational astronomy to specify $\Delta''_{1/2}$, i.e., the full width of a star image at the half maximum (FWHM). We omit further an upper symbol, measuring the image quality both in arcsec and microns. To distinguish Δ_{80} *for a telescope alone* from similar quantities, we designate it later as θ_{tel}.

For a Gaussian profile, we have approximately

$$\Delta_{80} \approx 1.269\,\Delta_{rms} \approx 1.524\,\Delta_{1/2}. \tag{1.1}$$

A word of caution is warranted against using $\Delta_{1/2}$ in cases where the profile of the image has a specific appearance. For example, sometimes it is a superposition of a relatively narrow central peak and a wide substrate, as it had a spot for the original Hubble Space Telescope. The same is particular to systems with rippled optical surfaces (O'Neill 1963, Chapter 6; Wetherell 1982; Suiter 1994, Chapter 13). In such cases, $\Delta_{1/2}$ and Δ_{80} may differ by several times, which is significant in the interpretation of photometric and spectroscopic observations.

Obviously, no strict definition for 'wide-field telescopes' exists; we merely propose a suitable working definition. For now, it is sufficient to consider a telescope as *wide-field* if its angular field of view, within which images of stars are not worse than a few arcsec, exceeds in size about 1°.

1.1.3 Efficiency of a survey

Along with a number of standard parameters of telescopes, it is useful to have a parameter that gives an idea of the efficiency of the telescope as a survey tool. To date, a widely used parameter is the *étendue*

$$E \equiv \pi w^2 \cdot \pi D_e^2/4, \tag{1.2}$$

a product of the observed sky area (deg^2) and the effective area of the telescope aperture (m^2). The *effective aperture* D_e takes into account the vignetting of useful light in the telescope, and with the significant role of this

3 The situation here resembles an old story about a woman who wanted to become a secretary. "Oh, can you really type at a rate of 200 words per minute?!" exclaimed the manager, looking at her resume. "Of course," the woman replied, "but it ends up as nonsense..."

factor it can be noticeably inferior to the *entrance pupil diameter* D.[4] For a conventional two-mirror telescope, we can use, as a good approximation, the relation

$$D_e \simeq D\sqrt{1-\eta^2}, \tag{1.3}$$

where η is the *linear obscuration coefficient*, which approximately equals the ratio of the diameters of the secondary and primary mirrors.

The inadequacy of the étendue with respect to the problem of interest is clear from the fact that E does not take into account the quality of images provided by a telescope. Meanwhile, there is no doubt that with better angular resolution, higher survey efficiency can be achieved.

An adequate measure of the survey efficiency, the *sky survey rate* Γ, is defined, up to a constant factor, as the ratio of the observed sky area πw^2 to the exposure time T needed to achieve the required S/N value (Terebizh 2011). It is not difficult to show (Appendix A) that such a definition leads to the following expression:

$$\Gamma \equiv \frac{\pi w^2 \cdot \pi D_e^2/4}{\theta^2} = E/\theta^2, \tag{1.4}$$

where θ is the so-called *delivered image quality*:

$$\theta \equiv \sqrt{\theta_{atm}^2 + \theta_{tel}^2 + p^2}, \tag{1.5}$$

and θ_{atm}, θ_{tel}, and p are the angular image sizes due to, respectively, atmospheric turbulence, telescope aberrations, and the finite size of the detector pixels. The first two of these parameters correspond to an 80% level of energy.

As expected, the image quality naturally entered into Eq. (1.4), and its influence is even more significant than the area of the aperture and field of view, because it is in the denominator of this expression. In essence, Γ is the product of the number of resolution elements in the observed region of the sky and the effective area of the telescope aperture.[5]

A convenient practical unit of measurement for the sky survey rate is

$$herschel \equiv 1\,\mathrm{m}^2\,\mathrm{deg}^2/\mathrm{arcsec}^2, \tag{1.6}$$

named after William Herschel (1738–1822). The rest of this book will use the abbreviation H for this unit.

4 The diameter of the paraxial image of the stop in object space. See Section 1.3.1.

5 Tonry (2011) proposed a more detailed approach to the evaluation of the survey efficiency, which includes consideration of the *point spread function* form and its alignment with the pixels of the detector.

1.1.4 Limiting stellar magnitude and survey speed

The notion of the *sky survey rate* Γ introduced above describes well the capabilities of the telescope itself, while the observer and the developer of a survey project also need the estimates of the stellar magnitude achievable with the instrument for a fixed exposure time and the corresponding survey speed. For our purposes, it is desirable to get sufficiently accurate values that are reasonably consistent with the observational data and, at the same time, do not enter into details that are superfluous in this context.

Such compromise calculations are given in Appendix A. We have for a limiting stellar magnitude:

$$m_{lim} = \mu/2 + 1.25\log_{10}(N_0 \cdot q \cdot U \cdot \delta\lambda \cdot \epsilon \cdot T) + 2.5\log_{10}[D/(\theta \cdot S/N)], \quad (1.7)$$

where

- μ (magnitude/square arcsec) is the sky surface brightness,
- N_0 (photons/sec cm^2 μm) is the photon flux from a star of zeroth magnitude,
- $q = q_{atm} \cdot q_{tel}$ is the total transparency, including the atmosphere and telescope,
- $U \simeq 1 - \eta^2$ is the fraction of unvignetted rays in a telescope,
- $\delta\lambda$ (μm) is the waveband width,
- ϵ (photo-events/photon) is the quantum efficiency of the detector,
- T (sec) is the exposure time,
- D (cm) is the telescope entrance pupil diameter,
- θ (arcsec) is the *delivered image quality* defined by Eq. (1.5), and
- S/N is the threshold signal-to-noise ratio adapted for observations.

It is sufficient for us to assume $N_0 = 1 \cdot 10^7$ photons/sec cm^2 μm in the visual region of the spectrum.

Values of m_{lim} according to Eq. (1.7) are in agreement with the estimates of the SIGNAL package created by the team of the *Isaac Newton Group of Telescopes* (http://catserver.ing.iac.es/signal/). However, we do not require the calculations to exactly match the real data, as our primary goal is to evaluate the comparative characteristics for the various types of optical systems.

As for the survey speed S, in the usual case, when the field of view has the form of a circle of diameter $2w$ (deg), and a square detector is inscribed into the field, we have

$$S = \frac{2w^2}{T + T_d}\,\mathrm{deg}^2/\,\mathrm{sec}\,, \quad (1.8)$$

where T_d (sec) is the 'dead time' (or 'slew time'), corresponding to telescope repositioning and data readout. Obviously, if the entire field of view is filled with a detector, then 2 should be replaced by π in Eq. (1.8).

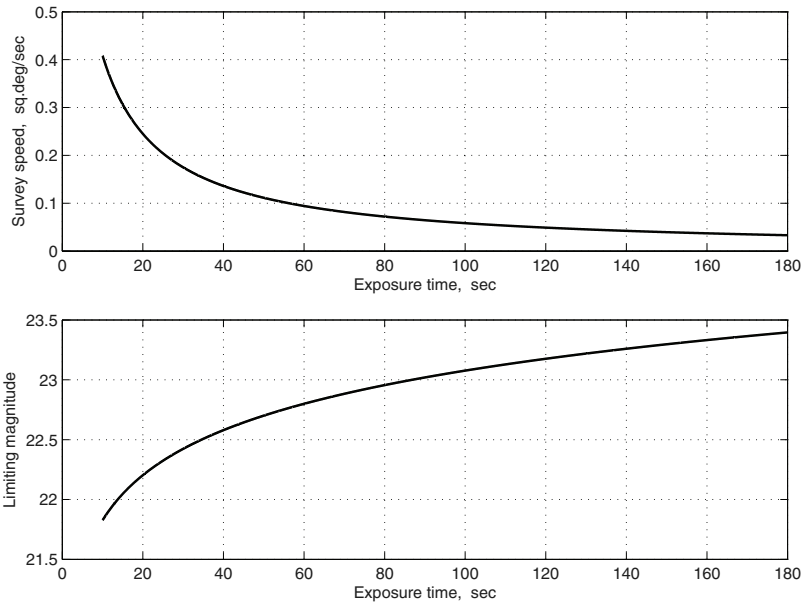

Figure 1.1 Limiting magnitude and survey speed as the functions of exposure time for the 1-m VT-056y design with a 3.5° field of view.

An example of functions $m_{lim}(T)$ and $S(T)$ is shown in Fig. 1.1. The design VT-056y represents a one-mirror telescope with a prime focus lens corrector (Terebizh 2016b). We assumed that $D = 1$ m, $F = 2.183$ m, $2w = 3.5°$, $q = 0.75$, $U = 0.85$, $\theta_{tel} = 0.65''$, $\theta_{atm} = 1.5''$, $\mu = 21^m$/arcsec^2, and the object zenith angle is 30°. The spectral bandwidth is 0.50 μm, and the dead time is 5 sec. As a detector, the STA1600 CCD with 10.56-$K \times$ 10.56-K pixels of 9-μm size was selected; its quantum efficiency $\epsilon = 0.85$. The threshold value $S/N = 7$ corresponds to the accepted field and detector sizes.

Naturally, as the exposure time increases, weaker objects are achievable; however, the loss of time for each exposure reduces the survey speed. Knowing the survey speed allows us to estimate the total time T_{obs}, which is required for viewing the sky area A (deg^2), namely, T_{obs} (sec) $= A/S$. The latter relation, together with Eq. (1.7) and Eq. (1.8), defines an important relationship between m_{lim}, S, and T_{obs}, in which the exposure time T serves as a convenient parameter. Thus, using such simple calculations, one can create the initial basics of a project, which will then be refined as the project details.

1.2 Cursory Review of Modern Wide-Field Telescopes

1.2.1 Large wide-field telescopes

Table 1.1 gives a list of 23 telescopes with an aperture diameter D larger than 1 m and a sufficiently wide angular field of view $2w$ (see also reviews of

Table 1.1 Wide-field telescopes with an aperture diameter D larger than 1 m. F is the effective focal length, and $2w$ is the field of view.

No.	Name	D (m)	F (m)	$2w$ (deg)	Optical system type
1	LSST	8.4	10.3	3.5	Paul + 3-lens corrector
2	Subaru HSC	8.2	18.7	1.5	5-lens prime focus corrector
3	SPM-Twin	6.5	29.3	2.0	3-lens Cassegrain corrector
4	DCT	4.2	9.7	2.0	6-lens prime focus corrector
5	VISTA	4.1	12.1	1.65	3-lens Cassegrain corrector
6	LAMOST	4.0	20.0	5.0	Reflective Schmidt
7	DESI	4.0	11.5	3.2	6-lens prime focus corrector
8	Blanco DECam	3.93	11.5	2.2	5-lens prime focus corrector
9	AAT	3.9	12.7	2.0	4-lens prime focus corrector
10	DSST	3.5	3.5	3.5	Paul + 3-lens corrector
11	WIYN ODI	3.5	22.1	1.4	2-lens Cassegrain corrector
12	VST	2.61	14.5	1.47	4-lens Cassegrain corrector
13	T250 ACTUEL	2.5	9.1	3.0	3-lens Cassegrain corrector
14	Steward 90″	2.3	6.83	1.1	4-lens prime focus corrector
15	SNAP	2.0	21.4	1.5	3-mirror Korsch
16	Pan-STARRS	1.8	8.0	3.0	3-lens Cassegrain corrector
17	KMTNet	1.6	5.2	2.8	4-lens prime focus corrector
18	SkyMapper	1.3	6.23	3.4	3-lens Cassegrain corrector
19	UKST	1.24	3.1	9.3	Schmidt
20	Oschin Schmidt	1.22	4.6	5.7	Schmidt
21	ESO Schmidt	1.0	3.1	6.4	Schmidt
22	OMI	1.0	2.5	3.11	4-lens prime focus corrector
23	GEODSS	1.0	2.2	2.1	3-lens prime focus corrector

Notes to Table 1.1

1. LSST: Large Synoptic Survey Telescope. Allsman et al. (2006), Ivezic et al. (2008), Gressler (2009).
2. Subaru HSC: Subaru Hyper Suprime Camera. Komiyama et al. (2010).
3. SPM-Twin: Spectroscopic telescope, San Pedro Martir NAO Mexico. Gonzalez (2007), Gonzalez and Orlov (2007).
4. DCT: Discovery Channel Telescope. MacFarlane and Dunham (2006). The DCT will also feature a Ritchey–Chrétien focus with a two-lens corrector.
5. VISTA: Visible and Infrared Survey Telescope for Astronomy. Ettedgui-Atad and Worswick (2003).
6. LAMOST: Large Sky Area Multi-object Fiber Spectroscopic Telescope. Cui et al. (2000).
7. DESI: Dark Energy Spectroscopic Instrument based on the Mayall 4-m telescope of KPNO. Martini et al. (2018), Miller et al. (2018).
8. Blanco DECam: Dark Energy Camera based on the Blanco 4 m telescope of CTIO. Kent et al. (2006), Flaugher et al. (2015).
9. AAT: Anglo-Australian Telescope. Jones (1994), Taylor and Gray (1990, 1994).
10. DSST: DARPA Space Surveillance Telescope. Curved focal surface. Grayson (2002).
11. WIYN ODI: WIYN Observatory One Degree Imager. Harmer et al. (2002).
12. VST: VLT Survey Telescope. Mancini D. et al. (2000).
13. T250 ACTUEL: Benitez et al. (2009), Cenarro et al. (2010).
14. Steward 90″ (Bok Telescope). Williams et al. (2004).
15. SNAP: Super-Nova Accelerating Probe. Lampton et al. (2002).
16. Pan-STARRS: Panoramic Survey Telescope and Rapid Response System (PS1). Kaiser et al. (2002), Hodapp et al. (2004), Morgan and Burgett (2009), Chambers et al. (2016).
17. KMTNet: Korean Microlensing Telescope Network. Kim, et al. (2010, 2011).
18. SkyMapper: Rakich et al. (2006).
19. UKST: United Kingdom Schmidt Telescope. Wynne (1981).
20. Palomar 48-inch Schmidt – Samuel Oschin Telescope has been upgraded at first to a Palomar Transient Factory (Law et al. 2009), and then to the Zwicky Transient Facility (Smith et al. 2014).
21. ESO Schmidt: Wilson (1996).
22. OMI: Canadian One-Meter Initiative. Roy (2010).
23. GEODSS: Two identical Ground-based Electro-Optical Deep Space Surveillance telescopes. Jeas and Anctil (1981).

Ackermann et al. 2010, Djorgovski et al. 2012). Strictly speaking, the purely spectroscopic telescopes SPM-Twin, LAMOST, and N. U. Mayall telescope with the DESI corrector should be considered separately. Some of the telescopes are not yet operational, but the current state of the projects is not considered here, since we are interested in the optics of wide-field telescopes itself. For the same reason, we are referring not only to existing telescopes but also systems for which non-trivial optical solutions were found but have not yet been implemented. An example is a three-mirror Korsch anastigmat with an aperture of 2.0 m and a 1.5° field of view proposed in the Super-Nova Acceleration Probe (SNAP) project. Readers interested in the results of the survey studies should turn to the discussion by Djorgovski et al. (2012).

In the following chapters, we describe some of the telescopes listed in Table 1.1 in more detail, namely, LSST (Section 3.3.1), Subaru HSC (Section 3.1.4), LAMOST (Section 2.2.5), Blanco DECam and Mayall DESI (Section 3.1.3), VST (Section 3.2.1), SNAP (Section 2.3.2), and Pan-STARRS (Section 3.2.2).

The $[D_e - 2w]$ diagram corresponding to the data in Table 1.1 is shown in Fig. 1.2. The effective diameter D_e values were evaluated according to Eq. (1.3).

The first thing to note in Fig. 1.2 is the especially large field sizes of the three Schmidt telescopes. This is exactly Schmidt's breakthrough. In the second half of the 20th century, sky surveys with Schmidt telescopes contributed most of the progress in extragalactic astronomy. It is enough to

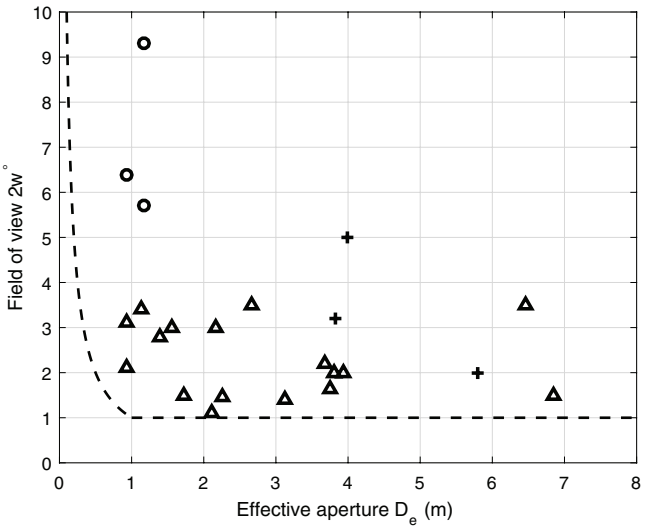

Figure 1.2 Effective aperture diameter (m) vs. angular field of view (deg) for the telescopes listed in Table 1.1. Spectroscopic telescopes are shown as crosses and Schmidt systems as circles. The dashed line separates the wide-field region according to Eq. (1.9).

recall the Palomar Sky Survey, made with the help of a 48-inch Schmidt camera, that served as the basis to identify extragalactic radio sources, which led, in particular, to the discovery of quasars.

Unfortunately, modern technology does not allow us to make lenses larger than about 1.5 m. Above this value, telescopes are distributed in the diagram more or less evenly in the 1.0−3.5° band, with the exception of the gap in the region of $D_e \simeq 5$ m. An important fact is the limit of the field size from above for the telescopes that don't belong to the group of Schmidt cameras and spectroscopic systems. Indeed, the area $2w < 3.5°$ is occupied by diverse mirror telescopes equipped with comparatively small lens correctors in a converging beam (Chapter 3), and it turns out that, regardless of the particular optical layout of a telescope, its angular field size is bounded above by the same value.

The simplest explanation of the latter fact holds that the angular field of view $2w \simeq L/F \simeq L/(\phi D)$ radians, where L is the linear size of the detector, and $\phi \equiv F/D$ is the *focal ratio*.[6] It is possible now to implement a *flat* field of a relative size $L/D \sim 1/10$, while ϕ has to be reduced to about 1.5–2.0 in order to simplify the optical design and to decrease the size of the telescope. Hence, an obvious way to further expand the field in large telescopes uses big detectors on a curved focal surface.

As regards the aforementioned lack of systems with an effective aperture of about 5 m, it seems to be a correctable omission. The efficiency of such systems would be sufficient to advance the problems mentioned in the Preface, while difficulties in manufacturing and operating, as well as cost, would be substantially reduced compared to those for larger telescopes. As an example of the systems in question, consider the design of the corrected Gregorian telescope, which is presented in Section 3.2.4.

With the commissioning in 2012 of Blanco DECam and Subaru HSC, wide-field observations reached a new level, characterized by a conjunction of depth of investigation and a large field of view. An analysis of such a vast flow of information assumes the joint efforts of consortiums of astronomers.

It is desirable sometimes to have, for cataloging purposes, a formal definition of a wide-field optical system. Figure 1.2 suggests the simple definition of a boundary that separates wide-field telescopes from the others:

$$2w^\circ = \begin{cases} 1/D_e & \text{if} \quad D_e \le 1\,\text{m}, \\ 1 & \text{if} \quad D_e > 1\,\text{m}, \end{cases} \tag{1.9}$$

where the field angle is measured in degrees and the effective diameter in meters.

6 In older sources, the focal ratio was denoted most often by *f*/#. We also use this designation sometimes, but only ϕ is used in the mathematical context.

Note that the Ritchey–Chrétien telescope with a field of nearly 20′ does not fall into the class of wide-field systems. Equation (1.9) gives reasonable estimates even for smaller apertures. For example, the field of view of a survey system should be not less than 10° for a 10-cm objective (such as a commercial *Canon 200* lens), $2w \geq 4°$ for a 25-cm camera, and $2w > 2°$ for a 0.5-m telescope.

1.2.2 Survey telescopes of moderate size

Just as a navy cannot be restricted to aircraft carriers only, in a survey case it is reasonable to distribute tasks between instruments with various apertures and field sizes. A substantial part of the survey data is now obtained using telescopes with a diameter of less than 1 m, and there are reasons to expect that wide-field telescopes of moderate size will be manufactured even after the commissioning of the Large Synoptic Survey Telescope.

The telescopes discussed would be presented in Fig. 1.2 in the domain $D < 1$ m, $2w < 50°$. Virtually all of these systems are successors of the classical Schmidt camera (Sections 1.3.3 and 4.1.1). From an optical point of view, the wide-field telescopes of moderate aperture have interesting variations in design, which is not possible in larger telescopes (see especially Köhler 1948, Buchroeder 1971). The basic information for these telescopes will be given in Chapter 4, along with descriptions of individual systems. This section discusses only some productive sky surveys aimed at finding near-Earth objects (NEOs), in particular, the potentially hazardous asteroids or comets with orbits that closely approach the Earth and are of a size large enough to cause significant regional damage in the event of impact.

The Catalina Real-Time Survey (Steward Observatory Station, Tucson, Arizona, USA) is a NASA-funded project supported by the NEOs Observation Program (Drake et al. 2009). The project utilized a 1.5-m *f*/2 telescope with a 1.1° field diameter and a 68-cm *f*/1.7 Schmidt telescope with a 3.4° field. In 2017, all operating observatories found a little more than 2,000 NEOs; almost half of them fell to Catalina Survey.

The Pan-STARRS survey (see Section 3.2.2), which uses the 1.8-m PS1 telescope with a field of 3.0°, provided about 43% of the total number of NEOs discovered in 2017.

One of the new projects is the Asteroid Terrestrial-impact Last Alert System (ATLAS), the first stage of which entered operation in 2015 (Tonry 2011, Tonry et al. 2018). This system, funded by NASA and developed by the University of Hawaii, comprises two observatories separated by about 100 km that simultaneously scan the complete northern sky every two days to a stellar magnitude fainter than 19. So far, each of the locations has one telescope with the Schmidt system, equipped with a three-lens focal corrector (Section 4.1.2); in the future, the number of observatories and telescopes is expected to increase. Table 1.2 shows the main characteristics of the base telescope.

Table 1.2 Specifications of the ATLAS Schmidt telescope.

Parameter	Value
Aperture	50 cm
Effective focal length	100 cm (*f*/2.0)
Field of view	7.5°
Detector	STA1600, $10.56K \times 10.56K$ CCD
Pixel size	9 μm (1.86″)
Effective PSF FWHM at 1.5″ seeing	2.5″
Nominal exposure time	30 sec
Readout time	6 sec

Since the ATLAS used previously made telescopes primarily to debug the software before moving on to new instruments, it was possible to optimize the entire observation channel, including the telescopes, their location, detectors, and data analysis. This ensures the opportunity to reach faint objects with telescopes of moderate aperture. Together with a high cadence, this makes the system an effective means of detecting new objects, as well as tracking variables and transient phenomena in the sky.

1.3 Some Attendant Issues of Optics

Although this book is devoted to the optical systems of telescopes, we will only briefly touch on the basic results of classical optics, since they are excellently described in fundamental monographs, starting with Born and Wolf (1999), Hecht (1998), G. Smith (1998), and Geary (2002) and ending with special handbooks on astronomical optics by Danjon and Couder (1935), Dimitroff and Baker (1945), Maksutov (1946), Wilson (1996, 1999), and Schroeder (2000). The purpose of this section is to focus on some issues of particular interest in the development of wide-field optical systems. In passing, this will allow us to avoid repetitions when discussing the seemingly different optical layouts.

1.3.1 Aperture stop and pupils

In optics, including its astronomical part, the concept of the system's *aperture stop* and the related concepts of *entrance* and *exit pupils* are of great importance (Born and Wolf 1999, Section 4.8.2).

The axial beam of light passing through the system is limited by the diaphragms, if they exist, and by the frames (or edges) of the optical elements, which can also be considered as diaphragms. The *aperture stop* is the diaphragm that limits the beam of light to the greatest extent. In other words, it determines the cross-section of the beam that forms the image. The *entrance pupil* is the image of the aperture stop created by the part of the optical system that precedes the stop; the *exit pupil* is the image of the aperture stop created by the

part of the system that follows the stop. Evidently, both pupils are mutual images of each other with the forward and backward rays. Like every image of a physical object (in our case, of the stop), pupils can be real or virtual.

These notions can be illustrated with an example of a two-mirror telescope in which the light beam coming from a star is bounded by the mounting of the primary mirror (Fig. 1.3). In this case, the mounting's edge coincides with both the aperture stop and the entrance pupil of a telescope. As seen in Fig. 1.3, the Cassegrainian convex secondary mirror forms a virtual exit pupil, which is placed before the secondary in the path of the incident light beam, whereas the concave secondary mirror of the Gregorian telescope forms a real exit pupil towards the primary mirror.

It is important to keep in mind, in connection with the subsequent discussion, that the focal surface of an optical system is illuminated in such a way that the light beams appear to originate from the system's exit pupil.

1.3.2 Curvature of the focal surface

For wide-field telescopes (and we are only interested in such systems), the curvature of the focal surface becomes particularly tangible. This aberration is usually called the *field curvature*; its effect on image quality is closely related to *astigmatism.* Both of these aberrations are proportional to the square of the field angle, that is, they increase rapidly with an increasing field.

In the presence of astigmatism, as is the case with the Ritchey–Chrétien two-mirror telescope, we have two focal surfaces—for tangential and sagittal sections of the light beams, respectively—and these surfaces are essentially curved (Born and Wolf 1999, Section 5.5.3). Two focal surfaces coincide if spherical aberration, coma, and astigmatism are eliminated, but, generally speaking, the common focal surface remains curved. This surface becomes a plane if, in addition, the *Petzval condition* is satisfied. The above is true only in the framework of the third-order theory of aberrations, which has limited value for wide-field systems.

In the context of astronomical observations, where the focal lengths are usually large, a significant angular field is combined with the large linear

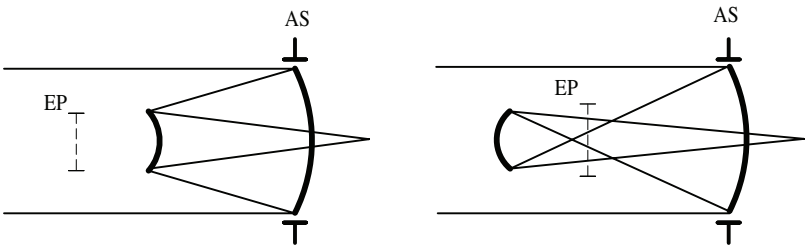

Figure 1.3 Positions of the aperture stop (AS) and exit pupil (EP) in the Cassegrain and Gregorian telescopes.

dimensions of the detector. This problem became imperative after Schmidt (1931) invented a camera with a field of view of about 10°. Until then, when calculating optical systems, the main goal was to achieve a flat focal surface to use common detectors. This approach is adopted in most of the systems considered in this book. Meanwhile, the field of view is sometimes so great that it should be left curved. It is time for us to understand that the curved focal surface is just as natural for telescopes as for the eyes of living beings.

The following ways seem to be preferred now in this regard: (i) the use of large detectors with a curved surface; (ii) applying the long-known technology based on a plurality of delicate waveguides with a curved-in-aggregate input surface (figured fiber-optic plates); and (iii) the faceting of the curved focal surface, i.e., the use of relatively small, flat detectors equipped with local field-flattening optics.

In the old days, either a photographic plate or a film were bent along a curved focal surface at wide-field observations, but these detectors are no longer used because of their low quantum efficiency. The principal issues and examples of modern curved detectors were discussed by Iwert and Delabre (2010) and Iwert et al. (2012); the first of these articles includes a photograph of a curved detector with a size of 60 mm × 60 mm and a curvature radius of 500 mm. There are also working examples of curved detectors of this type. In particular, a mosaic of curved detectors has been implemented in the DARPA-developed 3.5-m Space Surveillance Telescope (Blake et al. 2013).

The second option (figured fiber-optic plates) considered in a modern context involves a number of technological problems. The basic difficulties may be overcome within the framework of the program announced by the European Space Agency, which provides a solution for mapping a curved image field onto a flat imaging detector array.[7]

In connection with the third option, it is appropriate to mention the 95-cm Kepler space telescope with the equivalent field diameter of 11.6°. Its detector consists of 21 pairs of ordinary 59-mm × 28-mm CCDs covered by sapphire field-flattening lenses. An analogous procedure is applicable in other systems discussed here.

The future development of wide-field systems will be based on the first way, which involves the creation of large detectors with a curved surface.

1.3.3 'Ideal' wide-field telescope and Schmidt camera

The term 'ideal' was employed by Karl Strehl (1905) to describe the system in Fig. 1.4(a). The system is simple: it includes only a spherical mirror and a diaphragm located in the center of the sphere. A huge field of view is available

7 The details can be found in a note from 19 March 2013 at http://www.esa.int/Our Activities/Space Engineering & Technology/.

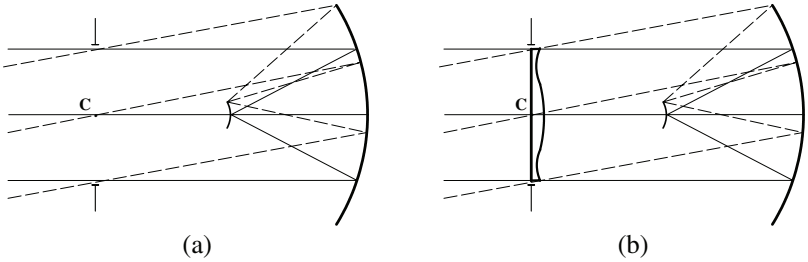

Figure 1.4 The two steps in the design of the Schmidt camera: (a) 'Ideal' telescope of Strehl. (b) Lens corrector at the center of curvature C.

to the system, since there is no accentuated optical axis in it: all of the beams passing through the center are equal. Therefore, the images of stars within the field are the same; they are located on a spherical surface approximately in the middle between the diaphragm and the mirror.

However, images in the 'ideal' telescope are far from perfect, because they are spoiled by *spherical aberration*. The latter consists in the fact that the rays from the edge zone of the wide light beam form the image closer to the mirror than the rays reflected from the central zone[8] (Fig. 1.5). The great invention of Schmidt (1931) was the design and creation of a single-lens corrector placed at the center of curvature of a spherical mirror [Fig. 1.4(b)]. The ordinary corrector is a glass plate with one surface that has a substantially aspheric shape to compensate for the spherical aberration of the mirror. Namely, the central part of the corrector acts as a positive lens, which shortens the focal length, while its outer part acts as a negative lens [see Figs. 1.4(b) and 1.5].

In such a way, a field of view of about 10° can be attained (Section 4.1.1). To properly assess this achievement, recall that the field of a classical telescope is only a few arc minutes. The essence of the new optical system was clearly expressed by G. H. Smith (1998, p. 380): "There is now point

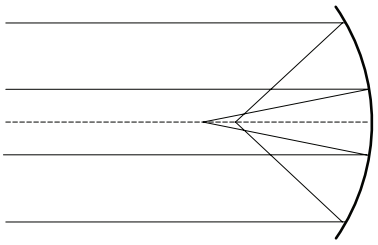

Figure 1.5 Spherical aberration of a spherical mirror.

8 Since spherical aberration can be characteristic of both spherical and aspheric optical elements, Maksutov (1946) considered it more appropriate to call it *zonal aberration on the axis.*

symmetry about the center of the stop (and the center of curvature of the mirror), rather than rotational symmetry about an axis. This point symmetry is the basis of the Schmidt telescope." Thus, the core of the centenary path from the 'ideal' telescope to the modern versions of the Schmidt camera can be summarized as follows:

> *The really wide field of view can be provided by placing an aperture stop at the center of curvature of the spherical mirror and subsequent correction of spherical aberration by elements of low optical power.*

Shortly after Schmidt's discovery, Maurice Paul (1935) used this approach to propose a three-mirror wide-field telescope, which is the basis of the most ambitious modern project, the Large Synoptic Survey Telescope (Sections 2.3.1 and 3.3.1). The core two-mirror subsystem in the Paul telescope, imitating the Schmidt corrector, is a Cassegrain telescope; a similar three-mirror generalization with a Gregorian core telescope was suggested by James Baker (see Dimitroff and Baker 1945).

The life of Bernhard Schmidt (1879–1935) and the history of his discovery are covered in a book by Mursepp and Weismann (1984) and articles of Wachmann (1955), Osterbrock (1994), and Busch, Ceragioli, and Stephani (2013). (Schmidt's mastery is all the more striking because he lost his right hand in his youth.) It is worth mentioning that Karl Strehl was not the first: the same system was discussed in the 19th century by Joseph Petzval and Hermann Vogel (Walter Stephani 2015, private communication). Strehl and Schmidt knew each other even before 1910. An important role in the spread of the new system was played by a young friend of Schmidt, Walter Baade, who prompted him to write a short article and later drew the attention of American astronomers to the extraordinary capabilities of a wide-field telescope. In the 1940s, Baade's studies at Mount Wilson Observatory led to a two-fold change in the estimation of the size of the known universe.

1.3.4 Remarks on color correction in catadioptric systems

Compensation of chromaticity in lens optics has been repeatedly described in the literature (see, e.g., Hecht 1998, Smith 1998, and, for historical perspective, King 1955). The paucity of a set of optical glass led Isaac Newton to doubt the possibility of compensating for this aberration in a lens-based system. Only a relatively recent study of Newton's diaries (Turnbull 1959, Whiteside 1969) revealed that his search for achromatic systems was more extensive than is commonly believed.[9] In 1673, Newton found another way to compensate for the longitudinal color of a single lens: by combining it with a meniscus lens-mirror, which was later named a *Mangin mirror.* The rays of different wavelengths are focused by a single lens

9 I am grateful to M. R. Ackermann, who has drawn my attention to this fact.

from blue to red in order of increasing distance from the lens, and in reverse order–by a Mangin mirror.

The corresponding telescope was patented much later by W. F. Hamilton (1814), so the systems like that shown in Fig. 1.6 with a separated lens/mirror-lens pair are known as *Hamiltonian telescopes*. The achromatic doublet of Chester Hall had already been well studied early in the 19th century, but flint glass was expensive, so Hamilton proposed the combination of a large crown lens with a smaller flint color-correcting element (Wilson 1996, p. 212). In fact, it is sufficient, and often preferable, to use the same type of glass for both elements.

Let us add that the known *medial* design by Schupmann (1899) introduces to the layout in Fig. 1.6 a small field element (a lens or a simple mirror) that projects an image of the front lens onto a correcting element in the form of a meniscus mirror-lens (Baker 1954, Daley 1984).

The above concerns only a change in the axial position of the focus depending on the wavelength, i.e., the *longitudinal chromatic aberration* (longitudinal color). In catadioptric systems, there is also the *lateral chromatic aberration* (lateral color, or more strictly, *chromatic difference of magnification*), and all of the "colored" varieties of monochromatic aberrations, among which we will distinguish *spherochromatism*. The lateral color is caused by the dependence of the effective focal length on the wavelength. As a result, images in different wavelengths have a different transverse scale. In particular, images of stars stretch radially into colored stripes whose length grows to the edge of the field of view. Spherochromatism means the dependence of spherical aberration on the wavelength. All types of chromatic aberrations, more or less distinct in simple optical systems, are intertwined with each other in wide-field telescopes in a fanciful way.

Nowadays, the Hamiltonian approach has led to elegant wide-field telescopes with closely sized optical elements; a detailed discussion will be given in Sections 4.2.3, 4.2.4, and 4.3.4. From a practical point of view, the production and use of Hamilton systems is somewhat more complicated than systems that contain conventional mirrors. Simple consideration shows that the free surface of the Mangin element should be made twice as accurately as

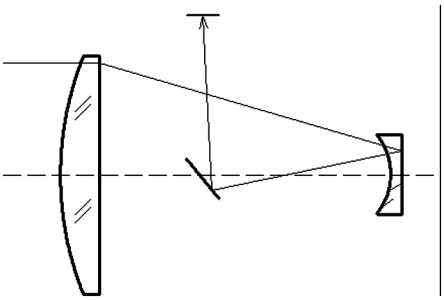

Figure 1.6 The W. F. Hamilton (1814) catadioptric system.

the surface of an ordinary lens, whereas the accuracy of the mirror's surface should be 6 times higher than the surface of the lens. This circumstance complicates the fabrication, but it also determines the tougher requirements for the temperature regime during both manufacturing and further operation.

In general, since most catadioptric telescopes have a high speed (low *f*/#), the correction of longitudinal chromaticity, and especially spherochromatism, constitutes a challenging problem. This task is often placed upon either a purely lens-based portion of the system or shared between the two components by the Hamiltonian method. Both ways have their difficulties, so it is useful to bear in mind an old recipe, which was summarized by Maxwell (1972, Section 2.1) as follows:

> *By locating the focal power in reflecting surfaces and the aberration correction in refracting components, the effects of chromatic aberration may be minimized.*

For example, both the Schmidt camera (Fig. 4.1) and the Richter–Slevogt system (Fig. 4.8) follow this rule. In the latter, a two-lens input corrector is essentially afocal, whereas a single lens in the Maksutov telescope (Fig. 4.7) has some optical power and as such needs to correct the spherical aberration of the primary mirror and compensate for its own chromatism simultaneously. For that reason, the two-lens corrector is better suited as a starting point for developing a wide field of view.

A good example of the potency of the described approach is an all-spherical system with a field of near-diffraction-quality images with an angular diameter of more than 45° (Terebizh 2016a). In particular, the four-lens corrector of one glass in the VT-119g model with a 30° field (Fig. 4.23) is nearly afocal (*f*/44), so chromatic aberrations are negligible.

1.3.5 Basic types of optical surfaces

Since the very first steps of optics, most optical surfaces have become conic sections. The reason for this is understandable, because it is the paraboloid that forms the perfect axial image of a distant star. Then the ellipsoid (in the Gregorian system) or the hyperboloid (in the Cassegrain system) transfers this image into a more convenient place while increasing the focal length.

The corresponding type of surfaces became *standard* in optical calculation programs. The equation of a conic section that has rotational symmetry about the z axis is

$$r^2 = 2R_0 z - (1 + b)z^2, \tag{1.10}$$

where $r = (x^2 + y^2)^{1/2}$ is the radial coordinate, R_0 is the paraxial radius of curvature, and the conic constant $b = -\epsilon^2$ is the negative squared eccentricity. It is suitable in optical ray tracing to solve Eq. (1.10) with respect to the surface sag z, so a standard surface is defined by

$$z = \frac{r^2/R_0}{1 + \sqrt{1 - (1+b)(r/R_0)^2}}. \tag{1.11}$$

The scarcity of the set of conic sections became increasingly clear as the field of view expanded, so a polynomial in the radial coordinate was added to the sag representation by Eq. (1.11). For example, an *even asphere* surface is defined as follows:

$$z = \frac{r^2/R_0}{1 + \sqrt{1 - (1+b)(r/R_0)^2}} + \alpha_1 r^2 + \alpha_2 r^4 + \ldots + \alpha_N r^{2N}. \tag{1.12}$$

In addition to the basic version, there are dozens of surface types in the developed programs of optical calculations. These surfaces are quite useful in practice, but limitations are apparent when we enlarge the system's aperture, speed, or the field of view. A power series slowly converges to a desired function (see, e.g., Lanczos 1988, Chapter 7; Press et. al. 1992, Section 5.1). In optics, we seek the most accurate approximation of a (maybe unknown) theoretically optimal surface profile, so we are greatly interested in a quickly converging series. Meanwhile, the convergence of the power series representation (Eq. (1.12)) is especially slow for the fast optical systems with a large aperture because it deals with powers of the ratio r/R_0, which is not particularly small near the edge of an aperture.

For these reasons, we can use another polynomial approximation to attain the higher speed of convergence, namely,

$$r^2 = 2R_0 z - (1+b)z^2 + a_3 z^3 + a_4 z^4 + \ldots + a_N z^N. \tag{1.13}$$

The coefficients $(a_3, a_4, \ldots, a_N)$, along with R_0 and b, define a polynomial representation of a surface in the sag z but not in the radial coordinate r. Even for fast surfaces, we usually have $z \ll r$, so the **poly**nomial expansion in the **sag**itta (*polysag*) is expected to converge more quickly than the series in Eq. (1.12). Besides, the direct extension of Eq. (1.10) in powers of the sag appears to be a more logical approach than adding a series in r powers to its solution with respect to the sag.

The generalization of the basic class of conic sections in the form of Eq. (1.13) has been known for a long time (see, e.g., Rusinov 1973), but as far as we know, it had never been applied systematically in optical design. For these reasons, the polysag surface type was added to the user-defined surfaces in ZEMAX (Terebizh 2008), so it becomes possible to use new surfaces with reflective and refractive optics.

The aspheric surface is usually tested with the help of an auxiliary optical device, a *null-corrector* (also called a *compensator*), which transforms the

reflected wavefront of the complicated form into the spherical wavefront (Wilson 1999, Section 1.3.4; Terebizh 2014). Since the null-corrector for a polysag surface would be designed in the same way as for a habitual asphere, the manufacturing of the polysag surfaces should not hold any surprises.

An example of the use of polysag surfaces will be given in Section 2.3.1. Of course, the properties of these surfaces deserve further study.

1.4 Matching of Optics and Detector with Atmospheric Image Quality

The practice of designing various telescopes shows that the desired optical layout essentially depends on the initial and final factors, i.e., the problems being solved and the given detector of light. The latter may seem less important, but keep in mind the importance of matching the resolving power of optics with that of the detector. Besides, the limited size of the detector often dictates the focal length of the telescope, and thus its speed and the optical layout itself. Finally, the optical layout of the wide-field telescope cannot be chosen independent of the supposed shape of the surface of the detector.

1.4.1 Detectors of light

Many publications are devoted to charge-coupled devices (CCDs) in optical astronomy, in particular, the *Handbook of CCD Astronomy* by Howell (2000); a later ESO Workshop *Detectors for Astronomy* (Oct. 2009) is also informative. Thus, it is inappropriate to discuss the topic extensively in this text. However, for proper matching of resolutions, the following typical characteristics of detectors should be taken into account:

- The spectral range. In wide-field observations, the designs are limited usually by the bandpass of the filters g (0.40–0.55 μm), r (0.56–0.69 μm), and i (0.69–0.82 μm). Regarding the optical calculations, the expansion of the waveband to the blue region is fraught with difficulties both in the selection of glass and the increase in the dispersion of light. Both difficulties are significantly mitigated when moving to the infrared region.
- The pixel size p. In detectors for wide-field observations, the most popular values are $p \simeq 9-15$ μm. Smaller values reduce the pixel's *full well capacity* (see below), whereas larger values impair resolution.
- The detector format, i.e., the number of pixels and the detector linear dimensions on both coordinates. In single-chip flat CCD detectors, the range for a format extends from 4096×4096 to 10560×10560 (STA1600) pixels. For a 9-micron pixel, this corresponds to linear dimensions of 36.9×36.9 mm and 95.2×95.1 mm, respectively; the

corresponding diagonal lengths are 52.1 mm and 134.5 mm. In calculations, detectors are usually assumed to be inscribed into the circular field of view of the telescope. Obviously, the dimensions of composite detectors can be very large. For example, in a DECam system with a 4.0-m aperture and a 2.2° field, a detector consisting of 15-μm pixels has a 45-cm diameter (Section 3.1.3). The linear diameter of the field of view of the Subaru Hyper Suprime Camera is 50 cm; it is even larger (64 cm) on the LSST.

- The *quantum efficiency* (QE) of the detector as a function of the wavelength, i.e., the average number of photo-events that one photon of a given wavelength causes. QE is noticeably different for the *front-illuminated* and *back-illuminated* CCDs. For the former, the peak QE is usually in the range of 55–60%, while for the latter it can reach 90% and even higher. For example, the QE of the E2V CCD 230-42 is 92% at 0.60 μm; the QE of the large-format STA1600 CCD is 87% at 0.60–0.65 μm.
- The full well capacity (FWC), i.e., the maximum number of events that a pixel can accumulate. Typically, the FWC of CCDs is in the range $(0.80 - 5.0) \times 10^5$ events. The larger the FWC is, the greater the dynamic range and the better the linearity of the detector.
- The dark current (DC), i.e., the average output signal in one pixel per hour at zero illumination. The dark current consists mainly of electrons thermally generated within the semiconductor material. For good back-illuminated CCDs, DC is less than 1 event/pixel/hour.
- The read-out noise, i.e., the random noise from the detector output stage in the absence of signal. A good value is considered to be several events (RMS) per reading.

So far we have only dealt with detectors of the CCD type. There are nearly the same CMOS-type (complementary metal-oxide semiconductor) light detectors, but they only recently began to compete with CCDs. Previously, CMOS detectors were too small, and they had insufficiently high quantum efficiency and unstable noise compared to scientific CCDs, but they read charge faster and had lower average readout noise. All mentioned shortcomings have been overcome now to a large extent, while preserving the merits (Zimmer, McGraw, and Ackermann 2016). In general, modern CCD and CMOS detectors have similar characteristics, so the choice of the detector depends on the specific problem being solved.

The present-day wide-field systems for telescopes of moderate and large size would be impossible without the rapid development of mosaic CCD technology. The latter provides a fairly quick reading of information from a set of CCDs with a total size of up to 1 m, whereas the gaps between the individual chips are negligible.

It is also worth adding that modern image detectors require a significant *back focal length* (BFL) for the telescope's optics, i.e., the distance from the

last optical surface to the light detector, especially accounting for the filter wheel, the focusing device, and the shutter. For wide-field telescopes with a moderate aperture, this can become a serious problem, the standard solution for which involves Newtonian or Cassegrainian image transfer outside the telescope tube.

1.4.2 Sampling factor

According to the Fourier theorem, almost every function can be represented as a superposition of harmonic oscillations of different frequencies, taken with due weight. If we are talking about a function of time, then the corresponding time frequency ν (cycles/sec) is inversely proportional to the time period of the harmonic oscillations. Similarly, the spatial frequency is defined as $f = 1/P$, where P is the period of the spatial harmonic of the function being studied, say, the image brightness distribution. Accordingly, the dimension of f is the number of cycles per unit length, usually cycles/mm.

The distributions encountered in practice often either do not change at a space scale smaller than some limit value a or high-frequency variations are not of interest. In other words, the spatial frequencies of real distributions are usually bounded from above by the value of the *cutoff frequency* $f_c \equiv 1/a$; such distributions are classified as the *functions of a bounded spectrum*.

Figure 1.7(a) shows a monochromatic distribution of brightness in the image of a star, i.e., the *point spread function* (PSF), which was obtained using the perfect paraboloid at zero vignetting of light. For ideal conditions, such as shown here, the PSF is called the *Airy pattern*. The radius of the central peak, known as an *Airy disk*, is $r_A \simeq 1.44\lambda\phi$, where λ is the wavelength, and $\phi \equiv F/D$ is the focal ratio; $r_A \simeq 2.9$ μm in this case. The Airy disk includes about 84% of all energy in the image of a point light source; thus, an Airy diameter of $2r_A$ is close to D_{80}. The spatial spectrum of the PSF, which is called the *modulation transfer function* (MTF), is identically equal to zero at frequencies above 500 c/mm in this example [Fig. 1.7(b)].

The last property is not an exception (Born and Wolf 1999, Section 9.5.2). The spatial spectrum of any, even perfect, optical system is bounded from above by the cutoff frequency

$$f_c = 1/(\lambda\phi), \tag{1.14}$$

i.e., of about the inverse Airy radius.[10] The reason for the strict cutoff of frequencies in optical systems is the diffraction of light, that is, due to its wave nature. Thus, when considering optical images, the minimum scale is $a = \lambda\phi$, and the cutoff frequency is $f_c = 1/a$. In the above example, we had $\lambda = 0.5$ μm and $\phi = 4.0$, so $f_c = 500$ c/mm.

10 If the wavelength is measured in microns, then f_c (cycles per mm) is $1000/(\lambda\phi)$.

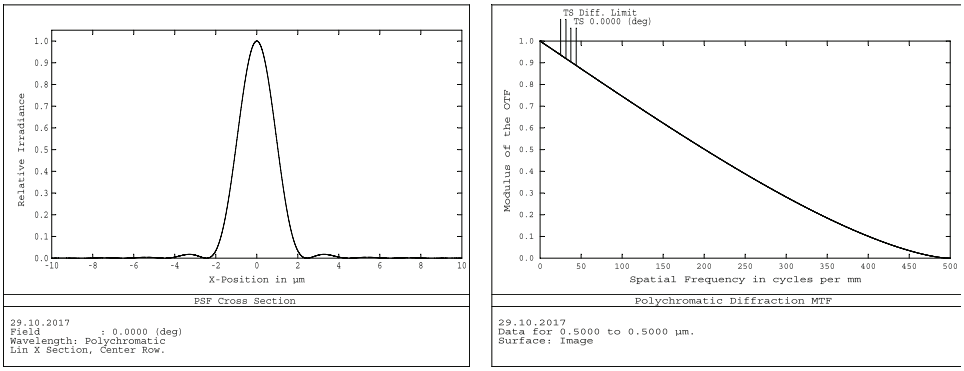

(a) (b)

Figure 1.7 (a) Cross-section of a PSF formed by perfect paraboloid (diameter = 1 m, focal length = 4 m) in monochromatic light with a wavelength of 0.5 μm. (b) Spatial spectrum of the PSF.

The continuous distributions are an idealization. In practice, we are dealing with discrete samples, most often made with some constant step δx. This leads to the appearance of a second characteristic frequency, called the *Nyquist frequency*:

$$f_{Ny} \equiv 1/(2 \cdot \delta x). \tag{1.15}$$

Comparative values of the two characteristic frequencies f_c and f_{Ny} determine the quality of the picture obtained as a result of the sampling of a continuous distribution.

According to the *sampling theorem* by E. Whittaker, V. Kotel'nikov, and C. Shannon (see, e.g., Press et al. 1992, p. 500), to completely restore a function of a bounded at some cutoff frequency f_c spectrum, the following condition must be met:

$$f_{Ny} \geq f_c, \tag{1.16}$$

or, equivalently, the sampling step

$$\delta x \leq 1/(2f_c) = a/2. \tag{1.17}$$

It is said sometimes that for a complete reconstruction of a function, the *sampling frequency* $f_s \equiv 1/\delta x = 2f_{Ny}$ must at least double the cutoff frequency. In optics, Eq. (1.17) takes the form

$$\delta x < \lambda\phi/2. \tag{1.18}$$

In the context of astronomical observations, sampling is specified by the pixel size p, so that the Nyquist frequency $f_{Ny} = 1/(2p)$, and Eq. (1.18) requires

that $p \le \lambda\phi/2 \simeq r_A/2$: *the pixel should be less than about half the Airy radius.* It is more convenient to write this inequality as

$$r_A/p \ge 2. \tag{1.19}$$

Images in telescopes, especially in wide-field ones, are by no means always diffractive. As said previously, the value of θ_{tel} characterizes the image quality provided by a telescope alone. Usually, it varies from about $0.5''$ up to a few arcsec, i.e., has the same order of magnitude as the typical atmospheric blurring θ_{atm}. For our purposes, it is enough to accept that the angular diameter of a star image due to these two factors is

$$\theta = \sqrt{\theta_{atm}^2 + \theta_{tel}^2}. \tag{1.20}$$

After setting the image quality, it is reasonable to generalize the above Eq. (1.19) as follows:

$$\chi \equiv \theta/p \ge 4, \tag{1.21}$$

where the ratio χ of the diameter of the star image to the pixel size is called the *sampling factor*. Thus, one usually should have at least 4 pixels covering the diameter of a star image. Taking into account random fluctuations of the light flux, this value is usually increased to 8 for precise photometric measurements (e.g., $\chi \simeq 7$ for the Kepler space telescope). On the other hand, for surveys where detecting faint objects is of primary importance, the sampling factor is reduced to 1–2.

For the design VT-056y that used as an example in Section 1.1.4 (Fig. 1.1), $\theta_{atm} = 1.5''$, $\theta_{tel} = 0.65''$, $p = 0.85''$, so $\theta = 1.63''$, and $\chi = 1.9$. Hence, the design is well suited to searching or exploratory observations.

Naturally, if the condition in Eq. (1.21) is violated, i.e., pixels are too rough, the object's image is irreversibly smoothed. In the frequency domain, this means that the spatial spectrum located above the Nyquist frequency is superimposed on the low-frequency region; this phenomenon is called *aliasing*.

In addition to sampling, further smoothing is caused by averaging over the pixel's area. The last factor is formally reduced to multiplying the original spectrum by $\mathrm{sinc}(pf)$, where the known function

$$\mathrm{sinc}(z) \equiv \sin(\pi z)/(\pi z), \quad -\infty < z < \infty. \tag{1.22}$$

The first positive zero of function $\mathrm{sinc}(pf)$ is at the frequency $f_{01} = 1/p$, so that smoothing due to the finite pixel size becomes significant at a frequency twice the Nyquist frequency.